Studies on Imidazolium-Based Ionic Liquids Having a Large Anion Confined in a Nanoporous Silica Gel Matrix

ARTICLE *in* THE JOURNAL OF PHYSICAL CHEMISTRY B · JUNE 2011

Impact Factor: 3.3 · DOI: 10.1021/jp2003358 · Source: PubMed

3 AUTHORS, INCLUDING:

Manish Pratap Singh
University of Aberdeen
26 PUBLICATIONS **205** CITATIONS

SEE PROFILE

THE JOURNAL OF PHYSICAL CHEMISTRY B

ARTICLE

pubs.acs.org/JPCB

Studies on Imidazolium-Based Ionic Liquids Having a Large Anion Confined in a Nanoporous Silica Gel Matrix

Manish Pratap Singh, Rajendra Kumar Singh,* and Suresh Chandra

Department of Physics, Banaras Hindu University, Varanasi-221005, India.

Supporting Information

ABSTRACT:

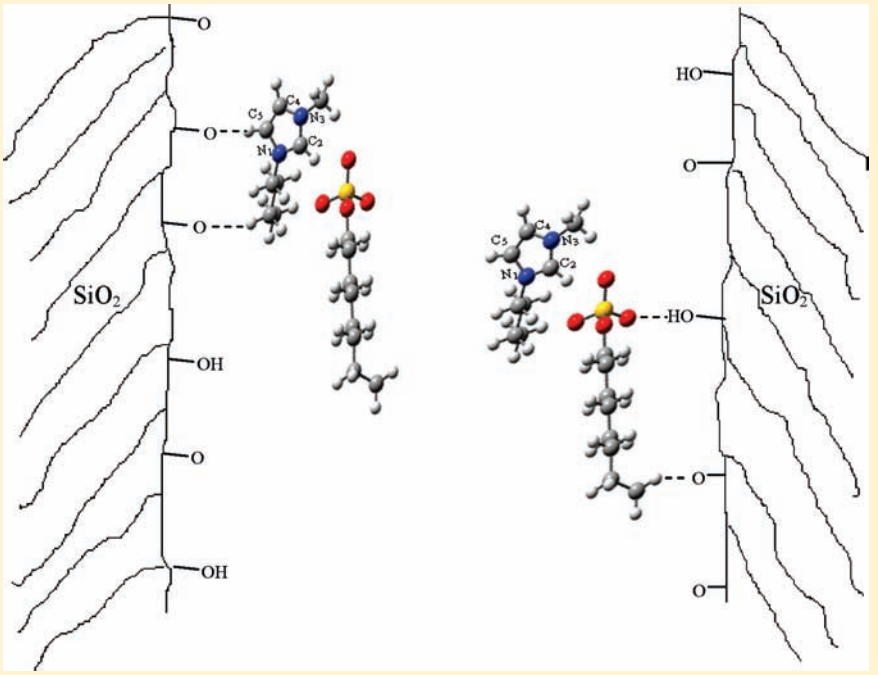

The properties of large molecules confined in nanopores are expected to be different from those of the bulk. This study reports changes in the phase behavior and vibrational frequencies of an imidazolium-based ionic liquid (IL), namely, 1-butyl-3-methyl imidazolium octyl sulfate ([BMIM][$OcSO_4$]) in a nanoporous silica gel matrix. Nanoporous silica gel matrixes have been synthesized by a one-step sol−gel technique using tetraethylorthosilicate (TEOS) as a starting precursor. The synthesized gel has been characterized by differential scanning calorimetry (DSC), BET, TEM and FTIR. The FTIR spectra show shifts in many vibrational bands; particularly, the vibrational bands related to the imidazolium ring, aliphatic chain, and SO_3 of the IL are found to shift significantly upon confinement. The DSC results show significant changes in the melting point ($\Delta T_m \approx 52$ °C), crystallization temperature ($\Delta T_C \approx 14$ °C), and glass transition temperature ($\Delta T_g \approx 2$ °C). The IL used in the present study has a large anion ([$OcSO_4$]), and ΔT_m for this is much larger than those reported earlier for many other ILs with relatively smaller anions. A new approach, based on the liquid-drop model, has been suggested to explain this.

INTRODUCTION

Ionic liquids (ILs) form a new class of materials that have self-dissociated cations and anions. ILs are composed of large organic cations and inorganic/organic anions of varying sizes.[1] The presence of dissociated cations and anions leads to high ionic conductivity in ILs.[2] Apart from high ionic conductivity, the ILs have a low vapor pressure, a large electrochemical window, high thermal stability, high chemical stability, and a wide liquidus range and good capability of dissolving various organic/inorganic materials.[2] The recyclability makes it an attractive alternative for use as less-polluting solvents in chemical synthetic processes.[3] Interesting electrochemical applications of ILs have been reported, namely, electrodeposition[4] and electrochemical devices (like batteries, fuel cells, super capacitors, electrochemical

Received: January 12, 2011
Revised: April 12, 2011
Published: May 18, 2011

solar cells, electrochromic devices,[2,5−8] etc). However, the use of ILs in devices becomes limited because of its liquidus nature, which leads to di culties such as packaging, leakage, portability, and so forth. To circumvent the problem of liquidus systems, our group suggested insertion of an ion-conducting salt solution into porous silica alcogels[9,10] long ago. Since the discovery of ILs, Dai et al.[11] for the first time introduced ILs in porous silica gels. Subsequently, these materials were termed as "Ionogels".[12] Now, ionogels are being extensively investigated by physicists, chemists, and material scientists.[12−16] Ionogels have been found to be suitable for many device applications such as optical solvents, sensors, biosensors, catalysis, biocatalysis, and so forth.[17] It may be noted that the very nature of ionogels involves entrapment of ILs in the confined geometry of nanopores. Therefore, it would be important to know the changes in the properties of ILs in a confined geometry. Many molecular liquids, liquid crystals, water, and so forth[18−21] are already reported to have different physicochemical properties in confined geometry. Because IL molecules are big, the confinement is likely to affect their properties much more. Many attempts have been made to study ILs in a confined geometry involving a wide variety of systems with different matrixes, pore sizes, pore wall surface functionalization, types of ILs, and so forth, as detailed below.

1. Matrix Pore Size. The extent of confinement is controlled by this factor. The pore wall interaction results in structural changes, which in turn will affect the phase transition,[15,16] optical properties,[22] conductivity,[23] and viscosity.[24] Direct measurement of some parameters like viscosity (η) is difficult. Kim and Dauskardt[24] used an indirect method of evaluating η from experimentally measured values of the diffusion coefficient (D), assuming the Stokes−Einstein relation $D \approx kT/\eta$. The diffusion coefficient in the confined geometry was measured using the lateral solvent diffusion technique.[24] They kept the liquid under study in contact with the edge of the porous matrix and monitored the mobility of the liquid by noting the change in the refractive index (or color) of the matrix as the liquid penetrated it. From this, the value of the diffusion coefficient (D) was evaluated.

2. Pore Wall Surface Decoration/Functionalization. Transition temperatures of confined ILs in functionalized silica pores are found to be widely different from that of nonfunctionalized silica pores.[25]

3. Type of Matrix. The confining matrixes could be "insulating" oxide matrixes SiO_2, SnO_2, and so forth or mesoporous "conducting" matrixes of silver, single-wall carbon nanotubes (CNTs), multiwall CNTs, and so forth.[12−16,22,25−40] The properties in oxide and conducting porous matrixes change differently because of the difference in the nature and extent of the IL−pore wall interaction. For example, the melting points have been found to decrease for many ILs when confined in a porous SiO_2 matrix,[12,13,16,22] while they increase when confined in porous conducting matrixes like silver,[15] CNTs, and so forth[27] because the former has a weaker IL−pore wall interaction than the latter. Apart from the ILs confined in pores, interesting changes in the phase behavior are also reported on the supported ionic liquid phase (SILP) by immobilizing or grafting the IL cation onto the surface of many insulating matrixes.[41]

4. Types of Cations/Anions in IL. Most studies of ILs in confined geometry are focused either on (a) the imidazolium-based cations like 1-ethyl-3-methyl imidazolium [EMIM], 1-butyl-3-methyl imidazolium [BMIM], 1-decyl-3-methyl imidazolium [DMIM], 1-cetyl-3-methyl imidazolium [CMIM], 1-hexyl-3-methyl imidazolium [HMIM], 1-hexadecyl-3-methyl imidazolium [HDMIM], 1-octyl-3-methyl imidazolium [OMIM], 2,3-dimethyl-1-octyl imidazolium [DMOI], and so forth or (b) pyridinium-based cation like 1-butylpyridinium [BPy], 1-butyl-4-methyl pyridinium [BMePy], and so forth. The associated anions were tetrafluoroborate [BF_4], hexafluorophosphate [PF_6], chloride [Cl], bromide [Br], bis-(trifluoromethanesulfonyl)imide [TFSI], dicyanamide [$N(CN)_2$], ethyl sulfate [$EtSO_4$], thiocyanate [SCN], methanesufonate [CH_3SO_3], triflate [TfO], and so forth.[12−16,22,23,25−40]

In our earlier experimental and theoretical studies on [BMIM][PF_6] confined in a silica matrix, we found that the cation ring becomes weakly attached to the silica pore wall surface, leading to changes in the melting point, uorescence, and vibrational bands.[22] It may be noted that all of the studies listed above, including our study,[12−16,22,25−40] were on ILs with small anions. We feel that, apart from the large cation of the confined IL, if the confined IL has a larger anion as well, then both the cations and anions may interact significantly with the pore wall of a confining matrix. As a result, it may show larger variation in the properties of the IL in the confined geometry. With this view in mind, an IL ([BMIM] [$OcSO_4$]) having a large anion ([$OcSO_4$]) has been chosen for the present study. Changes in the following properties of the IL in the confined geometry have been studied: T_c (crystallization temperature), T_g (glass transition temperature), T_m (melting point), cation ring-related vibrations, aliphatic chain C−H vibrations, and SO_3-related vibrations of the anion. Notably, we have found that for the present system with a large anion, the changes in T_c, T_g, T_m, or IR are much larger than those that have been observed earlier for confined ILs with small anions.[12−16,22,25−40]

MATERIALS AND METHODS

1. Chemical. The IL was procured from Sigma−Aldrich and used as received, except that it was vacuum-predried for 24 h at 100 °C. Ethyl alcohol (GR grade) and HCl were purchased from Merck Germany, while TEOS was procured from Sigma-Aldrich.

2. Synthesis of the IL Confined Porous Silica Gel. IL confined porous silica gels have been prepared using a similar procedure as that described by us[22] earlier. The IL chosen for the present study is [BMIM] [$OcSO_4$]. Care was taken in handling of IL so that it did not come into contact with ambient humidity (handled under a dry nitrogen atmosphere). Schematically, the method of preparation of the IL entrapped in SiO_2 is given in Figure S1 (see Supporting Information). All of the gel samples so obtained were vacuum-dried. Further, before any measurement, the samples were again heated at a temperature of 150 °C for 24 h in a vacuum of 10^{-3} Torr to remove traces of water. The gel was finally vacuum-dried. IL confined silica gels of $(100 - x)SiO_2 + x$IL for x = 0, 6.8, and 26.9 wt % were prepared. For estimating these wt %, the amount of SiO_2 obtainable from the mass of TEOS was first calculated by assuming complete hydrolysis/alkolysis and condensation. Knowing the mass added to the reaction vessel, the wt % of the IL in the ingot could then easily be calculated. It is observed that the silica gel matrix containing 26.9 wt % IL was gelated in 11 h, while for the silica gel matrix having a lower loading of IL, that is, 6.8 wt %, the gelation time was relatively large (about 35 h). This is a general observation for many systems. The IL has a surfactant character and decreases the surface tension of the sol−gel matrix.[37] A large amount of IL allows sol−gel particles to approach each other more easily without large barriers and, in turn, enhances the rate of condensation. Apart from the rate of condensation (or rate of gelation), the size of the pores also

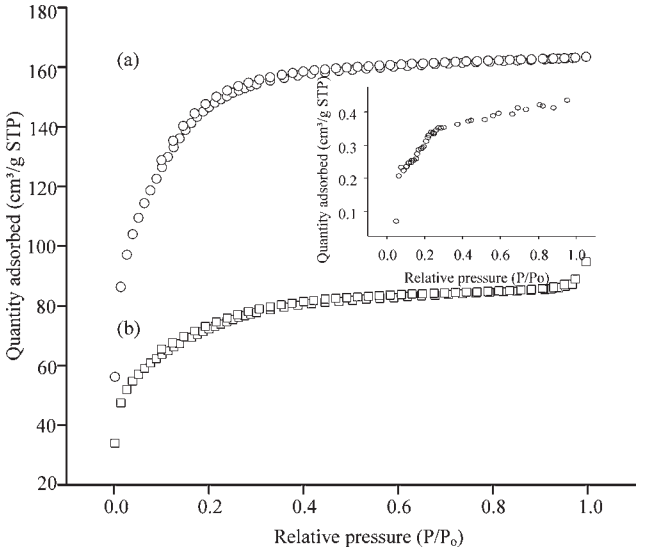

Figure 1. Nitrogen sorption isotherms of a silica-based gel matrix obtained from different loadings of IL [BMIM][$OcSO_4$] at 77 K, (a) 26.9 and (b) 6.8 wt % IL in a porous silica gel matrix. See the text for an explanation of the inset.

depends upon the IL loading (see ref 22 and other references cited therein).

3. Characterization Methods. *3.1. Transmission Electron Microscopy.* Transmission electron microscopy (TEM) was done on a Technai $20G^2$ model operated at 120 kV.

3.2. Pore Size Measurement. Nitrogen sorption experiments were carried out at 77 K on a Gemini VII 2390 t from Micromeritics Instrument Corporation. The surface area was measured by the BET (Brunauer−Emmett−Teller) method, while the average pore diameter was determined using the Barrett−Joyner−Halenda (BJH) approach. For BET analysis, the IL has to be extracted out before actual sorption measurements are carried out. For this, samples were soaked in dichloromethane at 60 °C for 2 h, and then, the solvent was thrown away. Again, the same process was used with acetone. This process was repeated three times to ensure proper washing of the IL in the matrix. In the final step of washing, samples were ultrasonicated in acetone. The filtrate was vacuum-dried for 12 h at 60 °C.

3.3. Differential Scanning Calorimetry (DSC). Phase transition temperatures of bulk and confined ILs were studied by DSC (Mettler Toledo DSC 1). The samples were first heated to 150 °C in situ and then cooled to −85 °C. Subsequently, the DSC thermograms were recorded at the heating rate of 10 K/min^{-1}.

3.4. X-ray Diffraction (XRD) Measurement. XRD patterns were recorded with a Philips X-ray diffractometer (PW-1710) using Cu Kα radiation. XRD patterns of silica gel with and without IL have been recorded.

3.5. Fourier-Transform Infrared (FTIR) Spectra. The FTIR spectra were recorded using a Varian 1000 FTIR Scimitar Series. The solid SiO_2/IL composite was dispersed in KBr and pelletized for recording the spectra of various SiO_2/IL samples. To record the spectra of the IL (neat), a drop of IL was used to wet the KBr pellet.

RESULTS AND DISCUSSION

1. Pore Analysis. The pore analysis is necessary to ascertain the manner in which the pore parameters (namely, diameter, pore volume, surface area, etc.) change in porous silica matrixes containing different loadings of the IL [BMIM][$OcSO_4$]. We carried out the BET analysis and nitrogen sorption isotherms, which are given in Figure 1. From Figure 1, it can be seen that the N_2 sorption isotherms exhibited a type-I-like behavior and are characteristic of micro- or supermicroporous materials according to the IUPAC classification.[42,43] The total pore volumes and surface areas of silica matrixes containing different amounts of IL in the reaction vessel are given in Table 1. The experimental pore diameter for pure silica (with out IL) is 3.0 nm,[22] while average pore diameters evaluated from the BJH model for samples with IL loading of 26.9 and 6.8 wt %, respectively, are 2.1 and 2.5 nm, which amounts to a change of nearly 20%. The higher the IL loading, the lower the pore diameter. Our earlier work on another IL ([BMIM][PF_6]) as well as many other studies has also shown the effect of IL loading on the pore diameter of the gel matrix.[22,32,36]

Table 1. Pore Volume, Surface Area, and Average Pore Diameter of Porous Silica Gel Matrixes Having Different IL Loadings

IL ([BMIM] [$OcSO_4$]) loading (wt%)	pore volume (cm^3/g)	surface area (m^2/g)	average pore diameter(nm)
0.0	0.64	843	3.0
6.8	0.14	241	2.5
26.9	0.25	485	2.1

It may be remarked that in the above discussion on the sorption isotherm, the IL from the sample was completely driven out before the BET measurement. In order to investigate whether the IL is physically confined in silica nanopores or just chemisorbed on the pore surface, we also carried out nitrogen adsorption measurements on a nanoporous silica gel matrix loaded with 26.9 wt % of IL (without removing IL). The result is shown in the inset of Figure 1. Comparing the results of nitrogen isotherms of a nanoporous silica gel matrix loaded with 26.9 wt % of IL and an IL extracted nanoporous silica gel matrix, we find that the pore volume (0.000168 cm^3/g) and quantity of N_2 adsorbed (0.4361 cm^3/g STP) are negligibly small as compared to the sample in which IL has been completely extracted out (see Figure 1), for which the pore volume was 0.25 cm^3/g and the quantity of N_2 adsorbed was 161.3567 cm^3/g STP. This clearly demonstrates that the IL is mostly physically confined in silica nanopores and the surface chemisorption is negligible.

Figure 2 shows a typical TEM image of the porous silica gel matrix loaded with 26.9 wt % of IL. The pore size estimated from TEM is about 2 nm. All of the results discussed later in this paper concerning the changes in the properties of the IL upon confinement are for the sample having a higher IL loading of 26.9 wt % in a silica matrix.

2. Change in the FTIR Bands of the IL upon Confinement. The surface of ideal unhydrolyzed silica matrix pore walls would have surface oxygen that can interact with the confined IL cation/anion end groups. However, in practice, some unintentionally (and unavoidably) hydrolyzed silica is always present. Thus, a complete study of the interaction of the IL should include its interaction with the oxygen and OH surface groups on the silica pore wall. We have theoretically optimized the structure of the IL cation−anion pair in the unconfined (or free) state using the Gaussian 03 package[44] by DFT calculation using the basis set B3LYP/6-31+g(d). Internal coordinates were generated using the Gauss View program,[45] which was used as input to the main

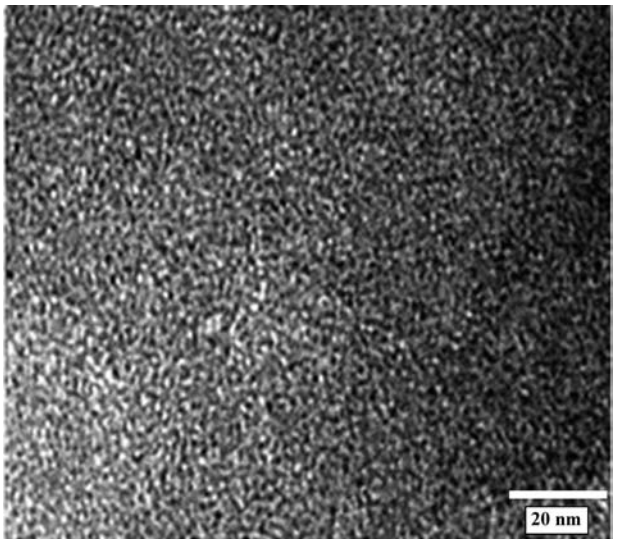

Figure 2. Typical TEM micrograph of 26.9 wt % IL loading in a silica gel matrix.

Gaussian program. A typical optimized geometry of [BMIM][$OcSO_4$] is given in Figure 3. It can be seen from Figure 3 that the hydrogen attached to the C_2 of the imidazolium cation ring prefers to come near the SO_3 of the octyl sulfate anion. If such a structure is confined in silica matrix nanopores, then both the cation and anion are likely to interact with surface oxygen (or OH) of the confining silica matrix wall. In turn, this will produce some dimensional changes in the interacting groups of the IL, resulting in changes of the vibrational frequencies related to the heterocyclic rings, aliphatic chain, as well as SO_3 group of the anion. Figure 4a shows schematically the manner in which an IL molecule would get incorporated inside of the nanopores of the silica matrix. The schematic representation of Figure 4a is guided by several molecular dynamics (MD) calculations, and experimental results available in the literature where there is possible alignment of IL molecules near the surface are discussed.[46−55] Sieffert and Wipff[46] have carried out MD simulations of an IL, namely, [BMIM][$OcSO_4$] near a quartz surface, and have concluded that the imidazolium ring and the octyl chain of the anion prefer to align near and parallel to the surface. Similar conclusions have been drawn experimentally by Baldelli et al.[47,48] They have also found that the cation and anion of the IL stack alternately. A similar type of stacking has been concluded by Dong et al.[49] for confinement in the CNT matrix. The proposed schematic representation given by us in Figure 4a is used to explain the changes in FTIR frequencies due to the IL−SiO_2 surface wall interaction. In Figure 4b, two typical cations and anions near the surface are drawn and discussed later. Figure 4b also shows the possible interacting sites, namely, (a) the OH group present on the silica surface interacting with the sulfate group of the anion, (b) the silica surface oxygen interacting with the end atoms of the long alkyl chain, and (c) the matrix surface oxygen interacting with the imidazolium ring of the [BMIM] cation. Therefore, the vibrational bands related to the sulfate group, alkyl chain, and imidazolium ring of the [BMIM] cation would be affected through the pore wall interaction. These expected changes were monitored by us using FTIR. The results are given below.

The FTIR spectra of a porous silica matrix, an unconfined (bulk) IL, and an IL confined in a porous silica matrix are shown in Figure S2 (see Supporting Information). For a detailed

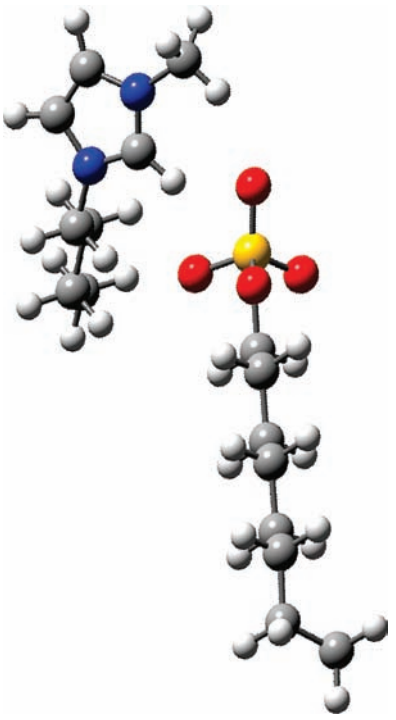

Figure 3. Typical preferred optimized geometry of [BMIM][$OcSO_4$] at B3LYP/6-31+g(d) level of DFT calculation. Carbon atoms are shaded gray, nitrogens are blue, oxygens are red, sulfur is yellow, and hydrogens atoms are white.

discussion of the effect of confinement on the spectra of the IL, we deconvoluted (using Peak fit v 4.12 for windows, copyright 2003) the selected regions of IR spectra corresponding to SO_3, C−H bands of the alkyl chain and cation ring vibrations for both confined and unconfined ILs. For selecting such regions, we were guided by our theoretical calculation and visual identification of vibrational bands using Gauss View. Assignments of such bands of interest are given in Table 2. From Table 2, it can be seen that the experimental data of the vibrational bands of the bulk IL agree reasonably with the computed frequencies. The difference between theoretical and experimental results is likely due to the anharmonicity effects.[56] The bands of the unconfined IL shift upon confinement as given below.

(i) From Figure 5, we can see that SO_3 related vibrational bands of an unconfined IL at 418 and 1166 cm^{-1} shift, respectively, to 415 and 1160 cm^{-1} upon confinement.

(ii) The cation ring C−H vibrations as well as $C_2-N_1-C_5$ vibrations also are affected because the ring is interacting with the pore walls, as shown earlier in Figure 4b. The imidazolium ring vibration of $C_2-N_1-C_5$ at 624 cm^{-1} (see Figure 5A) and those of the C−H vibration of the unconfined IL at 3121 and 3161 cm^{-1} (see Figure 6A), respectively, shift to 620, 3110, and 3152 cm^{-1} upon confinement.

(iii) The alkyl chain C−H vibrations at 2853, 2872, 2924, and 2963 cm^{-1} (see Figure 6B) of the unconfined IL shift to 2856, 2875, 2930, and 2961 cm^{-1}, respectively, upon confinement.

3. Phase Transition Temperatures of the IL Confined in a Silica Gel Matrix. The DSC thermograms of most ILs show three phase transition peaks, namely, (i) a first-order endothermic phase transition temperature corresponding to the melting point,

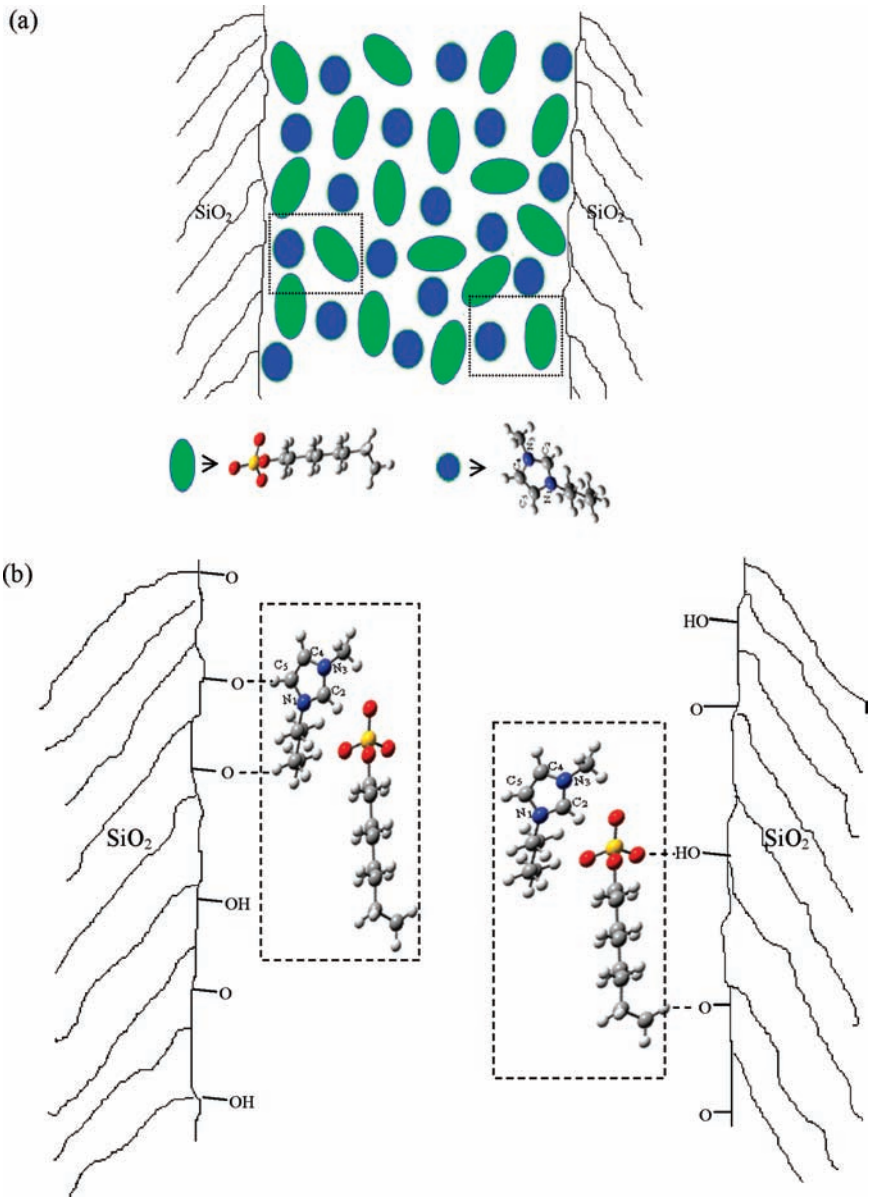

Figure 4. Schematic representation of (a) stacking of IL molecules inside of a nanoporous silica gel matrix. (b) Typical sites for interaction between an IL and a silica pore wall surface.

T_m (ii) a first-order exothermic phase transition temperature corresponding to the crystallization temperature, T_c and (iii) a second-order transition corresponding to the glass transition temperature, T_g. Depending on the thermal history of the sample, all three peaks may not be present, and one or two of these may be missed in the experiment. It is, therefore, generally imperative to keep the IL below T_g for a long time before starting the heating run. The DSC thermogram obtained by us for [BMIM][$OcSO_4$] is shown in Figure 7. The T_g, T_c and T_m are easily identifiable in Figure 7a for the unconfined (bulk) [BMIM][$OcSO_4$] sample, while for the confined IL, these peaks are relatively small because for the same mass of sample used in DSC, the "actual" amount of IL in the IL confined silica sample is much less than that in the IL sample. However, the credibility of the small DSC peaks comes from a careful look at the DSC thermogram of the confined IL, where we found the areas under the crystallization and melting peaks to be nearly the same, which is as expected in normal DSCs. The change in T_m that is, ΔT_m (= unconfined T_m − confined T_m), is 52 °C, while ΔT_c = 14 °C and ΔT_g = 2 °C. Note that our ΔT_m is positive, that is, the melting point decreases upon confinement. Some authors have reported an increase in ΔT_m upon confinement.[16,25,29] To reconfirm our results, we tried to find out by XRD the state of the IL ([BMIM][$OcSO_4$]) after confinement, which is expected to be liquid, as indicated from DSC results ($T_m \approx -18$ °C) given in Figure 7. The XRD of the silica gel with and without IL is given in Figure 8. We can see a broad "halo" in the 2θ region, 15−30°, showing the glassy nature of SiO_2 that remains preserved even after the incorporation of IL. It should be so because a confined IL has $T_m \approx -18$ °C and will be liquidus and will give no crystalline Bragg peaks of its own. Ultimately, it can lead to a slight broadening of the halo. In a pristine/amorphous SiO_2 matrix, the fwhm of the halo is 7.45°, which increases to 8.21°, as expected. Though it is small, it is enough to give credence to our conclusions. The

dx.doi.org/10.1021/jp2003358 |J. Phys. Chem. B 2011, 115, 7505–7514

Table 2. Experimental and Computed IR Frequencies of SO_3, $C_2-N_1-C_5$ Bending of the Imidazolium Ring, and C−H Stretching of the Aliphatic Chain As Well As the Imidazolium Ring of [BMIM][$OcSO_4$], Which Are Likely to Be Affected by Interaction with the Matrix Wall (see text)

experimental IR of [BMIM][$OcSO_4$] (cm^{-1})	theoretical IR of [BMIM][$OcSO_4$] (cm^{-1})	assignments
418	540	SO_3 antisymmetric deformation
624	666	out of plane bending of the $C_2-N_1-C_5$ in the imidazolium ring
1166	1232	SO_3 antisymmetric stretching
2853	3017	C−H stretching of the aliphatic chain
2872	3035	C−H stretching of the aliphatic chain
2924	3073	C−H stretching of the aliphatic chain
2963	3108	C−H stretching of the aliphatic chain
3110	3296	C−H stretching of the ring
3152	3314	C−H stretching of the ring

small peak at 44.5° is due to some SiO_2 crystallites (identified from JCPDS card no. 45-0131) present in an otherwise predominantly amorphous ingot. No solidus IL crystallite related peaks are observed, which tells that the confined IL is liquidus at room temperature, as also borne out by DSC results discussed earlier.

A comparison of ΔT_m, ΔT_c, and ΔT_g reported for some ILs confined in a silica matrix in relation to the present study is given in Table 3. It may be noted that ΔT_m for our case is very large (52 °C), while for other ILs, it varies from 2 to 20 °C. As pointed out earlier, the IL of the present study has a large anion as compared to other anions of ILs (shown in Figure S3, Supporting Information). It may be remarked that the smallest ΔT_m (2 °C) is observed for the smallest [PF_6] anion, while the largest ΔT_m of about 52 °C is for the largest anion studied. The results on the [BMIM]-cation-based ILs with largest anion [$OcSO_4$] (size ≈ 12.7 Å) and the smallest anion [PF_6] (size ≈ 3.3 Å) are from our laboratory (present study and ref 22, respectively). Values of ΔT_m for the [BMIM]-cation-based IL with [TFSI] anion of intermediate size (7.3 Å) are from Vioux et al.[29] Interestingly, not only the relative ion size but the ΔT_m for this is also intermediate to ΔT_m's of the ILs of smaller and larger anion sizes ([i.e., [PF_6] and [$OcSO_4$], respectively). Therefore, we have to seek an explanation for the change in transition temperatures that implicitly or explicitly takes the shape of the confined system into consideration. Most of the earlier conventional explanations for changes in ΔT_m suffered from the limitation of being not inclusive of shape dependence. We discuss below some of these and suggest the use of an alternate model of Nanda et al.[57] given for nanoparticles of different shapes/sizes.

4. Possible Explanations for Change in ΔT_m on Confinement. *4.1. Conventional Thermodynamic Formulations.* The most popular model applied earlier for explaining the phase behavior of confined ILs is due that of Gibbs−Thomson, based on classical

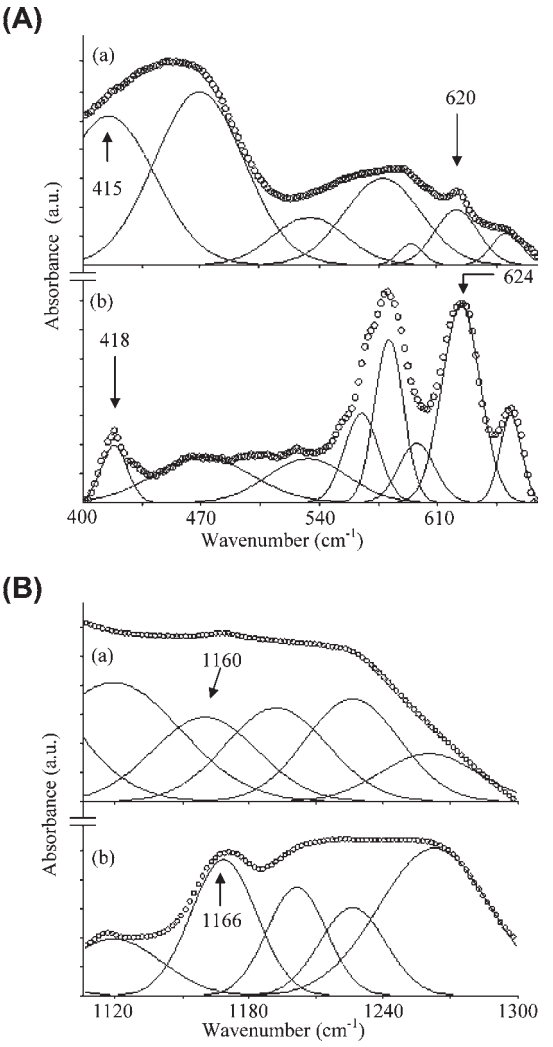

Figure 5. (A) Deconvoluted IR spectra of (a) a 26.9 wt % IL confined in a porous silica gel matrix and (b) an unconfined (bulk) IL (in the region of 400−670 cm^{-1}). (B) Deconvoluted IR spectra of (a) a 26.9 wt % IL confined in a porous silica gel matrix and (b) an unconfined (bulk) IL (in the region of 1100−1300 cm^{-1}).

thermodynamics. According to Gibbs−Thomson, a change in the melting point ΔT_m for a small crystal of diameter d is given as

$$\Delta T_m = T_m - T_m' = \frac{4\sigma_{sl} T_m V}{d\Delta H_f} \quad (1)$$

where σ_{sl} is the surface energy of the solid−liquid interface, T_m is melting point of unconfined crystals, T_m' is the melting point of crystals of diameter d, ΔH_f is the enthalpy of fusion (per gram−mole of unconfined material), and V is the molar volume of the liquid. There are many subsequent modifications[58−61] in the Gibbs−Thomson equation, which successfully interprets the change in melting point of small crystallites in confined geometry. For example, Couchman and Jesser[58] argued that the melting transition initiates on the surface of the confined particles and gave the following expression for the depression of melting point (ΔT_m)

$$\Delta T_m = T_m - T_m' = \frac{2\sigma_{sl} T_m V}{\Delta H_f (R - t)} = \frac{4\sigma_{sl} T_m V}{\Delta H_f (d - 2t)} \quad (2)$$

dx.doi.org/10.1021/jp2003358 |J. Phys. Chem. B 2011, 115, 7505–7514

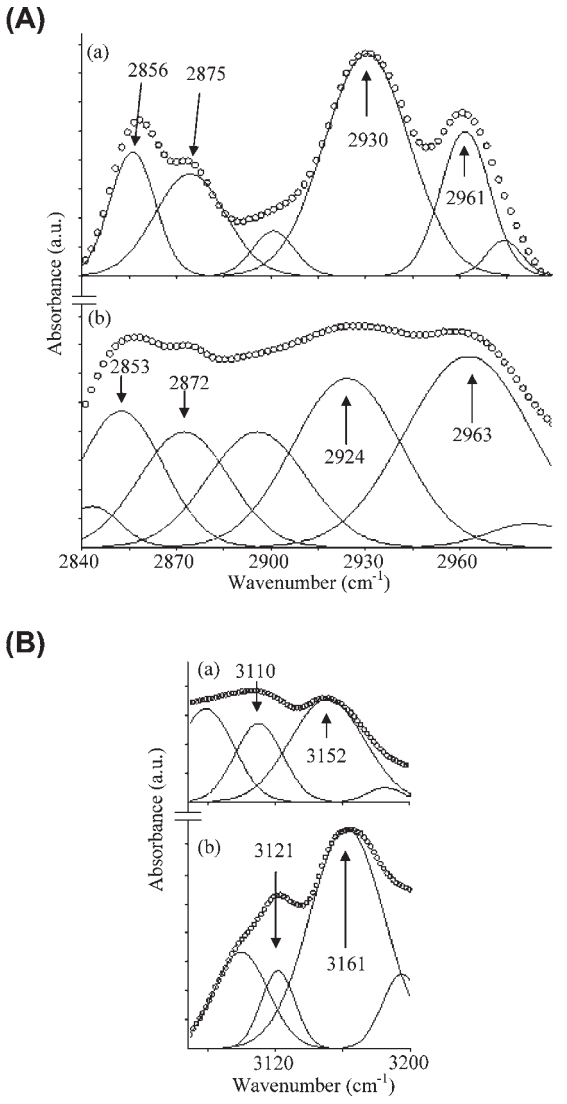

Figure 6. (A) Deconvoluted IR spectra of (a) a 26.9 wt % IL confined in a porous silica gel matrix and (b) an unconfined (bulk) IL (in the region of 2840−2990 cm^{-1}). (B) Deconvoluted IR spectra of (a) a 26.9 wt % IL confined in a porous silica gel matrix and (b) an unconfined (bulk) IL (in the region of 3070−3200 cm^{-1}).

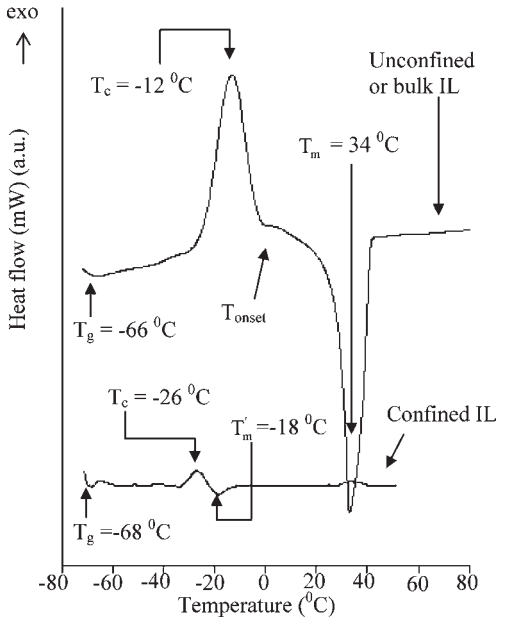

Figure 7. DSC thermogram of (a) an unconfined (bulk) IL and , (b) a 26.9 wt % IL confined in a porous silica gel matrix.

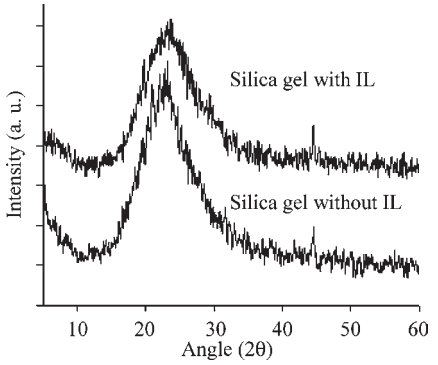

Figure 8. XRD of an as-synthesized silica gel with and without an IL.

where t is the thickness of the liquid around the solid particle. This is almost similar to the work of Warnock et al.,[59] and Faivre et al,[61] derived equation for ΔT_m for spherical and cylindrical pores and gave the general equation as

$$\Delta T_m = T_m - T_m' = \alpha \frac{2\sigma_{sl} T_m V}{\Delta H_f d} \quad (3)$$

where α is a constant whose value depends on experimental conditions; α = 2 and 3, respectively, for unstable and thermodynamic equilibria in spherical pores, and the corresponding values are 1 and 2 for cylindrical pores. All other symbols have the usual meaning. All of these equations suggest that a change in the melting point is inversely proportional to the diameter of the melting crystallites confined in the pore.

4.2. Mean Field Theory Approach. Mean Field Theory (MFT)[62] is another important model that has been used to explain the change in the melting point in a confined geometry. According to this model, melting point T_m' in a confined geometry is less than the bulk value, which can be explained by the following equation

$$T_m' = C\frac{\varepsilon Z}{k} \quad (4)$$

where C is a constant, Z is the mean coordination number for a molecule in the fluid, ε is the interaction energy with a nearest-neighbor molecule, and k is the Boltzmann constant. We,[22] as well as Neouza et al.,[12] applied this model to explain the phase transition of ILs in confined geometry.

All of the theories/models described above directly or indirectly assume the shape of the confined particle to be spherical, and nowhere does the shape of confined molecule enter explicitly. This may be required, particularly for ILs having large organic cations and anions. The above-discussed models as such cannot explain the dependence of ΔT_m on the anion size of the IL, as discussed earlier in the Results and Discussion section and summarized in Table 3. Here, we propose a new model based on Nanda et al.'s liquid drop model[57] given for the melting of the nanoparticles/low-dimensional system where the shape of the

Table 3. Change in the Transition Temperatures of Various ILs upon Confinement

S.N.	IL loading	preparatory method of the porous matrix	ΔT_m (°C)	ΔT_c (°C)	ΔT_g (°C)	length of the anion confined IL (Å)
1.	[BMIM][$OcSO_4$]	sol−gel; alkolysis	52	14	2	12.7
2.	[BMIM][TFSI]	sol−gel; nonhydrolytic	20[a]	20[a]	0[a]	7.3
3.	[EMIM][$N(CN)_2$]	sol−gel; alkolysis	15[b], 14[c]	−5[b], −4[c]	0[b,c]	4.4
4.	[BMIM][PF_6]	sol−gel; alkolysis	2[d]			3.3
5.	[EMIM][TfO]	sol−gel; alkolysis	9[b]	0[b,c]	−2[b, e]	3.0
6.	[EMIM][$EtSO_4$]	sol−gel; alkolysis	*e*	*e*	−1[c]	4.8

[a] Reference 29. [b] Reference 25. [c] Reference 16. [d] Reference 22. [e] Not observed in the reference in footnote [c].

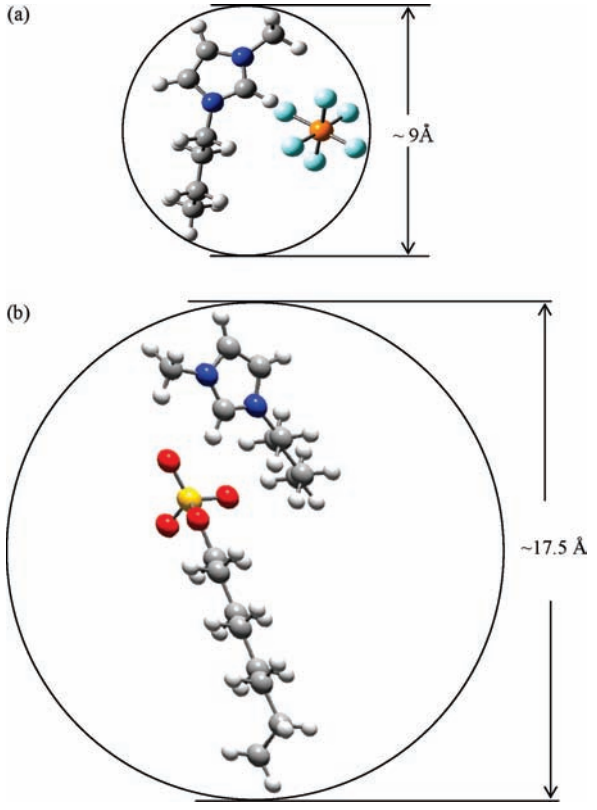

Figure 9. "Excluded steric volumes" for two ILs, (a) [BMIM][PF_6] with small anion [PF_6] and (b) [BMIM][$OcSO_4$] with large anion [$OcSO_4$].

confined species is taken into consideration implicitly. It is the intention of this paper to use this formulation to explain our results on the change in the melting point for ILs.

4.3. Shape-Dependent Changes in Melting Temperatures (Present Proposed Model). Recently, an interesting model for the melting of a nanoparticle/low-dimensional solid has been given by Nanda et al.[57] They draw an analogy between the melting of a nano or low-dimensional solid and the liquid drop model (originally given for Nucleus) and argue that "the properties of nanoparticles are dominated by surface atoms; therefore, their binding energy can be effectively represented by the volume and surface dependent terms as in the liquid drop model". Nanda et al. have used some simple ideas; namely, (i) a universal relationship exists between surface energy (a_s) and the cohesive energy (a_v). Further, the surface energy and melting temperature are correlated. The higher the surface energy, the higher the melting temperature. (ii) The most interesting feature of the above-said model is the manner in which the liquid drop model has been used to calculate the cohesive energy per atom ($a_{v,d}$) and correlate it with the melting temperature. According to the liquid drop model,[63] the total cohesive energy $\{E_{total}(N)\}$ of a cluster/nanoparticle of N atoms is given as

$$E_{total}(N) = \text{volume energy} - \text{surface energy}$$
$$= a_v N - a_s N^{2/3} \quad (5)$$

where a_v = cohesive energy of the bulk, $a_s = (4\pi r_a^2)\gamma$; r_a is atomic radius, and γ is the coefficient of the surface energy (see ref 52). The number of atoms (N) in a spherical nanoparticle of diameter d' is given by

$$N = d'^3/8r_a^3 \quad (6)$$

From eqs 5 and 6, we can obtain the total cohesive energy per atom as

$$a_{v,d} = \frac{E_{total}(N)}{N} = a_v - a_s N^{-1/3} = a_v - 6\gamma v_0/d' \quad (7)$$

Taking experimental data for a large number of elemental nanoparticles, it has been shown by Nanda et al.[57] that a_v and $a_{v,d}$ bear a similar linear relationship with T_m (the melting temperature of the bulk system) and T'_m (the melting temperature of the nanosystem), respectively, as given below

$$\left.\begin{aligned} a_v &= \psi \cdot T_m + C \\ a_{v,d} &= \psi \cdot T'_m + C \end{aligned}\right\} \quad (8)$$

where ψ and C are constants. Using eqs 7 and 8, we can write

$$\left.\begin{aligned} T'_m &= T_m - \frac{6v_0\gamma}{\psi d'} \\ \Delta T_m &= T_m - T'_m = 6v_0\gamma/\psi d' = \beta'/d' \end{aligned}\right\} \quad (9)$$

where $\beta' = 6v_0\gamma/\psi$ for a given system. This equation suggests that ΔT_m is proportional to $1/d'$ and also proportional to v_0 and γ. The term d' is the diameter of the cluster, which will be related to the diameter of the pore. Hence, for this term, the smaller the pore, the larger the ΔT_m . The shape of the molecule forming the cluster enters through the term β' (see eq 9). In eq 9, $v_0 = 4/3\pi r_a^3$, where r_a is the atomic radius in the theory of Nanda et al. given for atomic clusters. In our case, the IL molecule is the cluster-forming species, and hence, we assume v_0 to be associated with the "excluded steric volume" of the IL molecule, as shown in the Figure 9 for two ILs, namely, [BMIM][PF_6] with small anion [PF_6] and [BMIM][$OcSO_4$] with large anion [$OcSO_4$]. From the geometry given in Figure 9, the radii corresponding to the excluded steric volume for the larger anion containing [BMIM][$OcSO_4$] and the

dx.doi.org/10.1021/jp2003358 |*J. Phys. Chem. B* 2011, 115, 7505–7514

smaller anion containing [BMIM][PF_6] are about 8.7 and 4.5 Å, respectively. From eq 9, we get

$$\frac{\Delta T_{m_{[BMIM\ [OcSO_4}}}{\Delta T_{m_{[BMIM\ [PF_6}}} = \frac{(8.7)^3}{(4.5)^3} \quad 7.28$$

Thus, we can see that ΔT_m for the IL with a large anion, that is, [$OcSO_4$], will be more than 7 times that for [BMIM][PF_6]. This partly (but not fully) explains the high value of ΔT_m obtained by us for [BMIM][$OcSO_4$] in comparison to that of [BMIM][PF_6] (see Table 3). Therefore, we have also to consider the effect arising out of the different values of the surface energy (γ) for two ILs. The surface energy gets modified due to the pore wall interaction (see the Materials and Methods section and Figure 4). We have experimentally observed that in the [BMIM][$OcSO_4$] system, apart from the interaction of the ring, the tail of the alkyl chain as well as the SO_3 group of the anion interacts with the surface of the pore wall. These interactions will modify the surface energy term γ and hence enhance the value of ΔT_m. The above discussion shows that the combined effect of the size of the IL and the resulting modification in the surface energy changes the melting point by a large factor for the IL with a large anion.

Apart from the change in the melting point T_m, the T_c and T_g were also found to change upon confinement, though these changes were relatively less, as given in Table 3. The crystallization temperature T_c involves a very complex phenomenon involving the ability of the molecular system to supercool in the bulk form, molecular motions, the crystal wall interaction, and so forth. Nevertheless, whenever the crystallization temperature is found in a glass-forming liquid system, the pattern of ΔT_m and ΔT_c (or ΔT_g) is expected to be similar. Here also, ΔT_c and ΔT_g have been found to decrease (like ΔT_m), though the magnitudes are less. The observed T_g for the bulk IL ([BMIM][$OcSO_4$]) is about −66 °C, which decreases to about −68 °C. There is a decrease of 2 °C in ΔT_g upon confinement. Because the ΔT_g was very small, we repeated DSC many times to confirm the observed decrease in T_g. The decrease in the glass transition temperature can be explained on the basis of following Ehrenfest relation[64] given for the glass transition temperature in a confined geometry

$$\frac{dT_g}{dP} = T_g V \frac{\Delta\alpha}{\Delta C_p} \quad (10)$$

Combining this with the Kelvin equation[65] for an idealized cylindrical pore, the pressure reduction on the liquid inside of the pore compared with the vapor pressure can be written as

$$\Delta P = \frac{2\Delta\sigma}{R} \quad (11)$$

The resulting equation for a change in the glass transition temperature (T_g) of the IL in a confined geometry can be written as

$$\Delta T_g = \frac{V\Delta\alpha\, T_g 2\Delta\sigma}{R\Delta C_p} \quad (12)$$

where V is the molar volume, $\Delta\alpha$ is the thermal expansion coe cient, $\Delta\sigma$ is the difference between gas wall and liquid wall interfacial energies, ΔC_p is the heat capacity at constant pressure, and T_g is the glass transition temperature of the unconfined IL. Equation 12 does qualitatively explain the decrement in terms of $\Delta\sigma$, but it does not elucidate the manner in which gas wall and liquid wall interactions come into play. Fehr and Lowen[66] have done molecular dynamical calculations for liquids confined between two parallel plates using a soft sphere model. However, their calculations could not explain the experimental results of a change in T_g upon confinement for many organic liquids. They also surmised that the reason for the decrement in T_g is because of complicated wall−particle interactions. In the case of a strong wall−particle repulsive interaction, which has an attractive part also near the wall, a dense layer of particle will accumulate (and even freeze into a triangular crystal) in equilibrium. Hence, the rest of the system becomes less dense. Therefore, the density in the remaining layers is smaller. Therefore, it is expected to be the glass transition temperature may gets shifted to lower temperature.

CONCLUSION

In summary, we have studied the effect of confinement of an IL [BMIM][$OcSO_4$] (which has a large anion) in a nanoporous silica gel matrix. Upon confinement of the IL, a large shift is found in its vibrations related to the imidazolium ring, while significant changes are also observed in the C−H related vibrations of the aliphatic chain and the SO_3 related vibrations. Apart from changes in vibrational frequencies of the IL upon confinement, we have also found significant changes in phase- transition temperatures. Particularly, the change in melting point (ΔT_m) is very large as compared to that of confined ILs with smaller anions. A new explanation based on the liquid drop model given for melting of the nanocluster[57] is proposed where the size of the "confined IL" enters implicitly.

ASSOCIATED CONTENT

Supporting Information. Schematic representation of the different steps involved in IL confined nano porous silica gel matrix preparation, IR spectra of pure SiO_2 with bulk and confined IL and structural geometries of various anions. This material is available free of charge via the Internet at http://pubs.acs.org.

AUTHOR INFORMATION

Corresponding Author

*E-mail: rksingh_17@rediffmail.com. Tel.: +91 542 2307308. Fax: +91 542 2368390. Address: Ionic Liquid and Solid State Ionics Laboratory, Department of Physics, Banaras Hindu University, Varanasi-221005, India.

ACKNOWLEDGMENT

One of us (S.C.) is thankful to the National Academy of Science, India, for the award of the position of Platinum Jubilee Senior Scientist. (R.K.S.) is thankful to the DST, New Delhi, India, for providing financial assistance for carrying out this work under an award of DST Project No. SR/S2/CMP-71/2007. M.P. S. is thankful to CSIR, New Delhi, India. for an award of Senior Research Fellowship (SRF).

REFERENCES

(1) For reviews on the topic of ILs, see: (a) Handy, S. T. *Curr. Org. Chem.* **2005**, *9*, 959. (b) Welton, T. *Chem. Rev.* **1999**, *99*, 2071. (c) Armand, M.; Endres, F.; MacFarlane, D. R.; Ohno, H.; Scrosati, B. *Nat. Mater.* **2009**, *8*, 621. (d) Wasserscheid, P.; Keim, W. *Angew. Chem., Int. Ed.* **2000**, *39*, 3772. (e) Wasserscheid, P.; Keim, W. *Angew. Chem.* **2000**,

112, 3926. (f) Davis, J. H., Jr.; Fox, P. A. *Chem. Commun.* **2003**, *11*, 1209. (g) Hapiot, P.; Lagrost, C. *Chem. Rev.* **2008**, *108*, 2238. (h) Seddon, K. R. *Nat. Mater.* **2003**, *2*, 363. (i) Blanchard, L. A.; Hancu, D.; Beckman, E. J.; Brennecke, J. F. *Nature* **1999**, *399*, 28. (j) Dupont, J.; de Souza, R. F.; Suarez, P. A. Z. *Chem. Rev.* **2002**, *102*, 3667.

(2) *Electrochemical Aspects of Ionic Liquids*; Ohno, H., Ed.; John Wiley & Sons, Inc.: Hoboken, NJ, 2005.

(3) *Ionic Liquids in Synthesis*; Wasserscheid, P., Welton, T., Eds.; Wiley-VCH Verlag GmbH & Co. KGaA: New York, 2007; Vol. I.

(4) Al-Salman, R.; Endres, F. *J. Mater. Chem.* **2009**, *19*, 7228.

(5) Wishart, J. F. *Energy Environ. Sci.* **2009**, *2*, 956.

(6) Wang, P.; Zakeeruddin, S. M.; Moser, J. E.; Humphry-Baker, R.; Gratzel, M. *J. Am. Chem. Soc.* **2004**, *126*, 7164.

(7) Sun, J.; MacFarlane, D. R.; Forsyth, M. *Solid State Ionics* **2002**, *147*, 333.

(8) Cha, E. H.; Lim, S. A.; Park, J. H.; Kim, W. D.; MacFarlane, D. R. *J. Power Sources* **2008**, *178*, 779.

(9) Srivastava, R.; Chandra, S. *Phys. Status Solidi A* **2002**, *191*, 202.

(10) Srivastava, R.; Chandra, S. *Solid State Ionics* **2002**, *152*, 741.

(11) Dai, S.; Ju, Y. H.; Gao, H. J.; Lin, J. S.; Pennycook, S. J.; Barnes, C. E. *Chem. Commun.* **2000**, 243.

(12) Neouze, M.-A.; Le Bideau, J.; Leroux, F.; Vioux, A. *Chem. Commun.* **2005**, 1082.

(13) Neouze, M.-A.; Le Bideau, J.; Gaveau, P.; Bellayer, S.; Vioux, A. *Chem. Mater.* **2006**, *18*, 3931.

(14) Lunstroot, K.; Driesen, K.; Nockemann, P.; Gorller-Walrand, C.; Binnemans, K.; Bellayer, S.; Le Bideau, J.; Vioux, A. *Chem. Mater.* **2006**, *18*, 5711.

(15) Neouze, M.-A.; Litschauer, M. *J. Phys. Chem. B* **2008**, *112*, 16721.

(16) Göbel, R.; Hesemann, P.; Weber, J.; Moller, E.; Friedrich, A.; Beuermann, S.; Taubert, A. *Phys. Chem. Chem. Phys.* **2009**, *11*, 3653.

(17) Vioux, A.; Viau, L.; Volland, S.; Le Bideau, J. *C.R. Chim.* **2010**, *13*, 242.

(18) Findenegg, G. H.; Jähnert, S.; Akcakayiran, D.; Schreiber, A. *ChemPhysChem* **2008**, *9*, 2651.

(19) Hansen, E. W.; Stocker, M.; Schmidt, R. *J. Phys. Chem.* **1996**, *100*, 2195.

(20) Dosseh, G.; Xia, Y.; Alba-Simionesco, C. *J. Phys. Chem. B* **2003**, *107*, 6445.

(21) Shao, Y.; Zerda, T. W. *J. Phys. Chem. B* **1998**, *102*, 3387.

(22) Singh, M. P.; Singh, R. K.; Chandra, S. *ChemPhysChem.* **2010**, *11*, 2036.

(23) Davenport, M.; Rodriguez, A.; Shea, K. J.; Siwy, Z. S. *Nano Lett.* **2009**, *9*, 2125.

(24) Kim, T. K.; Dauskardt, R. H. *Nano Lett.* **2010**, *10*, 1955.

(25) Göbel, R.; Friedrich, A.; Taubert, A. *Dalton Trans.* **2010**, *39*, 603.

(26) Bellayer, S.; Viau, L.; Tebby, Z.; Toupance, T.; Le Bideau, J.; Vioux, A. *Dalton Trans.* **2009**, 1307.

(27) Wu, G.; Sha, M.; Huang, S. *J. Am. Chem. Soc.* **2007**, *129*, 2416.

(28) Echelmeyer, T.; Meyer, H. W.; van Wüllen, L. *Chem. Mater.* **2009**, *21*, 2280.

(29) Neouze, M.-A.; Le Bideau, J.; Vioux, A. *Progs. Solid State Chem.* **2005**, *33*, 217.

(30) Zhang, J.; Zhang, Q.; Shi, F.; Zhang, S.; Qiao, B.; Liu, L.; Ma, Y.; Deng, Y. *Chem. Phy. Lett.* **2008**, *461*, 229.

(31) Singh, M. P.; Singh, R. K.; Chandra, S. *J. Phys. D: Appl. Phys.* **2010**, *43*, 092001.

(32) Zhang, J.; Zhang, Q.; Li, X.; Liu, S.; Ma, Y.; Shi, F.; Deng, Y. *Phys. Chem. Chem. Phys.* **2010**, *12*, 1971.

(33) Le Bideau, J.; Gaveau, P.; Bellayer, S.; Neouze, M.-A.; Vioux, A. *Phys. Chem. Chem. Phys.* **2007**, *9*, 5419.

(34) Shi, F.; Zhang, Q.; Li, D.; Deng, Y. *Chem.—Eur. J.* **2005**, *11*, 5279.

(35) Shi, F.; Deng, Y. *Spectrochim. Acta, Part A* **2005**, *62*, 239.

(36) Karout, A.; Pierre, A. C. *J. Non-Cryst. Solid* **2007**, *353*, 2900.

(37) Oter, O.; Ertekin, K.; Derinkuyu, S. *Mater. Chem. Phys.* **2009**, *113*, 322.

(38) Lunstroot, K.; Driesen, K.; Nockemann, P.; Hecke, K. V.; Meervelt, L. V.; Gorller-Walrand, C.; Binnemans, K.; Bellayer, S.; Viau, L.; Le Bideau, J.; Vioux, A. *Dalton Trans.* **2009**, 298.

(39) Sha, M.; Wu, G.; Liu, Y.; Tang, Z.; Fang, H. *J. Phys. Chem. C* **2009**, *113*, 4618.

(40) Karout, A.; Pierre, A. C. *J. Sol—Gel Sci. Technol.* **2009**, *49*, 364.

(41) Vangeli, O. C.; Romanos, G. E.; Beltsios, K. G.; Fokas, D.; Kouvelos, E. P.; Stefanopoulos, K. L.; Kanellopoulos, N. K. *J. Phys. Chem. B* **2010**, *114*, 6480.

(42) Sing, K. S. W.; Everett, D. H.; Haul, R. A. W.; Moscou, L.; Pierotti, R. A.; Rouquerol, J.; Siemieniewska, T. *Pure Appl. Chem.* **1985**, *57*, 603.

(43) Rouquerol, J.; Avnir, D.; Fairbridge, C. W.; Everett, D. H.; Haynes, J. H.; Pericone, N.; Ramsay, J. D. F.; Sing, K. S. W.; Unger, K. K. *Pure Appl. Chem.* **1994**, *66*, 1739.

(44) Frisch, M. J.; Trucks, W.; Schlegel, H. B.; Scuseria, G. E.; Robb, M. A.; Cheeseman, J. R.; Zakrzewski, V. G.; Montgomery, J. A., Jr.; Stratmann, R. E.; Burant, J. C.; Dapprich, S.; Millam, J. M.; Daniels, A. D.; Kudin, K. N.; Strain, M. C.; Farkas, O.; Tomasi, J.; Barone, V.; Cossi, M.; Cammy, R.; Mennucci, B.; Pomelli, C.; Adamo, C.; Clifford, S.; Ochterski, J.; Petersson, G. A.; Ayala, P. Y.; Cui, Q.; Morokuma, K.; Rega, N.; Salvodar, P.; Dannenberg, J. J.; Malick, D. K.; Rabuck, A. D.; Raghavachari, K.; Foresman, J. B.; Cioslowski, J.; V.Ortiz, J.; Baboul, A. G.; Stefanov, B. B.; Liu, G.; Liashenko, A.; Piskorz, P.; Komaromi, I.; Gomperts, R.; Martin, R. L.; Fox, D. J.; Keith, T.; Al-Laham, M. A.; Peng, C. Y.; Nanayakkara, A.; Challacombe, M.; Gill, P. M. W.; Johnson, B.; Chen, W.; Wong, M. W.; Andres, J. L.; Gonzalez, C.; Head-Gordon, M.; Replogle, E. S.; Pople, J. A. *Gaussian 03*, revision A.1; Gaussian Inc.: Pittsburgh, PA, 2003.

(45) Dennington, R., II; Keith, T.; Millam, J.; Eppinnett, K.; Hovell, W. L.; Gilliland, R. *Gauss View 03*; Semichem, Inc.: Shawnee Mission, KS, 2003.

(46) Sieffert, N.; Wipff, G. *J. Phys. Chem. C* **2008**, *112*, 19590.

(47) Santos, C. S.; Baldelli, S. *J. Phys. Chem. B* **2007**, *111*, 4715.

(48) Aliaga, C; Santos, C. S.; Baldelli, S. *Phys. Chem. Chem. Phys.* **2007**, *9*, 3683.

(49) Dong, K.; Zhou, G.; Liu, X.; Yao, X.; Zhang, S.; Lyubartsev, A. *J. Phys. Chem. C* **2009**, *113*, 10013.

(50) Atkin, R.; Warr, G. G. *J. Phys. Chem. C* **2007**, *111*, 5162.

(51) Fitchett, B. D.; Conboy, J. C. *J. Phys. Chem. B* **2004**, *108*, 20255.

(52) Romero, C.; Baldelli, S. *J. Phys. Chem. B* **2006**, *110*, 6213.

(53) Pinilla, C.; Del Popolo, M. G.; Kohanoff, J.; Lynden-Bell, R. M. *J. Phys. Chem. B* **2007**, *111*, 4877.

(54) Rollins, J. B.; Fitchett, B. D.; Conboy, J. C. *J. Phys. Chem. B* **2007**, *111*, 4990.

(55) Hayes, R.; El Abedin, S. Z.; Atkin, R. *J. Phys. Chem. B* **2009**, *113*, 7049.

(56) Koch, W.; Holthausen, M. C. *A Chemist's Guide to Density Functional theory*, 2nd ed.; Wiley-VCH: New York, 2001.

(57) Nanda, K. K.; Sahu, S. N.; Behera, S. N. *Phys. Rev. A* **2002**, *66*, 013208.

(58) Couchman, P. R.; Jesser, W. A. *Nature (London)* **1977**, *269*, 481.

(59) Warnock, J.; Awschalom, D. D; Shafer, M. W. *Phys. Rev. Lett.* **1986**, *57*, 1753.

(60) Denoyel, R.; Pellenq, R. J. M. *Langmuir* **2002**, *18*, 2710.

(61) Faivre, C.; Bellet, D.; Dolino, G. *Eur. Phys. J. B* **1999**, *7*, 19.

(62) Hill, T. L. *Statistical Mechanics, Principles and Selected Applications*; McGraw-Hill: New York, 1956, Chapter 7.

(63) Naher, U.; Bjornholm, S.; Frauendorf, S.; Garcias, F.; Guet, C. *Phys. Rep.* **1997**, *285*, 245.

(64) Davies, R. O.; Jones, G. O. *Adv. Phys.* **1953**, *2*, 370.

(65) *Surface Tension and Absorption*; Defay, R., Prigogine, I., Eds. Wiley: New York, 1966.

(66) Fehr, T.; Lowen, H. *Phys. Rev. E* **1995**, *52*, 4016.